K isomerism in ^{255}Rf and total kinetic energy measurements for spontaneous fission of ^{255,256,258}Rf

P. Mosat, F.P. Hessberger, S. Antalic, D. Ackermann, B. Andel, M. Block, S. Hofmann, Z. Kalaninova, B. Kindler, M. Laatiaoui, et al.

K isomerism in ^{255}Rf and total kinetic energy measurements for spontaneous fission of ^{255,256,258}Rf

P. Mosat,[1,*] F. P. Heßberger,[2,3] S. Antalic,[1] D. Ackermann,[4] B. Andel,[1,5] M. Block,[2,3,6] S. Hofmann,[2,7] Z. Kalaninova,[1,8] B. Kindler,[2] M. Laatiaoui,[2,3] B. Lommel,[2] A. K. Mistry,[2,3] J. Piot,[4] and M. Vostinar[4]

[1]*Department of Nuclear Physics and Biophysics, Comenius University in Bratislava, 84248 Bratislava, Slovakia*
[2]*GSI Helmholtzzentrum für Schwerionenforschung, GmbH, 64291 Darmstadt, Germany*
[3]*Helmholtz-Institut Mainz, 55099 Mainz, Germany*
[4]*GANIL, 14076 Caen Cedex 5, France*
[5]*KU Leuven, Instituut voor Kern- en Stralingsfysica, B-3001 Leuven, Belgium*
[6]*Johannes Gutenberg-Universität Mainz, 55128 Mainz, Germany*
[7]*Institut für Physik, Goethe-Universität Frankfurt, 60054 Frankfurt, Germany*
[8]*Laboratory of Nuclear Problems, JINR, 141980 Dubna, Russia*

(Received 28 August 2019; revised manuscript received 3 January 2020; accepted 11 February 2020; published 23 March 2020)

Spontaneous fission properties of the isotopes ^{255}Rf, ^{256}Rf, and ^{258}Rf produced in the reactions ^{50}Ti + ^{207}Pb, ^{50}Ti + ^{208}Pb, and ^{50}Ti + ^{209}Bi were studied. The method of time and position correlations was used to identify spontaneous fission events. The correction to the energy deficit in measured total kinetic energy (TKE) determined on the basis of a study of ^{252}No was applied to evaluate the $\overline{\text{TKE}}$ of investigated rutherfordium isotopes. A signature which we assigned tentatively to bimodal fission was observed in TKE distributions of ^{255}Rf and ^{256}Rf. Two new high-K isomeric states in ^{255}Rf were identified by ER-CE-(CE)-α/SF correlation search, with half-lives of 38^{+12}_{-7} and 15^{+6}_{-4} μs at excitation energies 1150–1450 and 900–1200 keV, respectively. Including those metastable states a tentative partial level scheme was proposed.

DOI: 10.1103/PhysRevC.101.034310

I. INTRODUCTION

The spontaneous-fission process is believed to finally terminate nuclear stability. In the region of the heaviest elements, the macroscopic part of the fission barrier vanishes at $Z = 100$–104 and the nuclear stability against spontaneous fission (SF) is provided only by microscopic effects of few MeV resulting from the nuclear shell structure [1]. Investigation of structure and decay properties of the heaviest nuclei is essential in order to determine the production possibilities of superheavy isotopes, to understand the limits of nuclear stability, and to improve models predicting the next spherical proton and neutron shells beyond ^{208}Pb ($Z = 82$, $N = 126$). The study of spontaneous-fission features such as the relation of total kinetic energy (TKE), prompt neutron emission, and partial half-lives of the competing decay modes for isotopes in the transfermium region is mandatory to advance the understanding of this complex nuclear process [2].

In this region only some limited experimental information on half-lives or branching ratios is available; the knowledge concerning fission modes, kinetic energy release, and fission fragment mass distribution is scarce. Especially interesting are TKE measurements, that are connected to the fission mode (asymmetric from elongated shape, symmetric from elongated or compact shape). The experimental values of mean TKE ($\overline{\text{TKE}}$) as well as TKE distributions are very valuable inputs for the development of advanced SF theory.

The discovery of bimodal fission was achieved by measuring TKE distributions for a number of trans-uranium nuclides. Theoretical calculations discuss the possibility of bimodal fission for the even isotopes $^{254–260}$Rf, for which indications should be found in their TKE distributions [3]. In lighter nuclei in the fermium-nobelium region (^{258}Fm, ^{259,260}Md, and ^{258,262}No), experimental studies of mass and TKE distributions could confirm the concept of bimodal fission [4,5]. In all five reported cases of bimodally fissioning isotopes, one common feature was observed: the lower-energy fission mode was positioned at 200 MeV and the higher-energy fission mode at 233 MeV. Until now, only a few TKE measurements with limited statistics of SF events were performed for rutherfordium ($Z = 104$) isotopes [4–6].

In this work we present data on SF of ^{255}Rf, ^{256}Rf, and ^{258}Rf obtained at SHIP, where SF fragment energies of nuclei implanted in a silicon detector were measured. For the evaluation of the mean TKE release during the fission process it was necessary to correct the detector response for the energy deficit, mainly due to the pulse-height defect.

Another interesting feature studied in this region is the presence of isomeric states. In deformed, axially symmetric nuclei, the quantum number K is defined as the projection of total nuclear spin Ω onto the symmetry axis. By breaking nucleon pairs, multi-quasiparticle (qp) configurations with high K values are possible (typically 2-qp or 4-qp configuration for even-even and 3-qp for odd-even or even-odd isotopes).

*pavol.mosat@fmph.uniba.sk

TABLE I. Summary of the individual irradiations during the experiment. E_{targ} is the beam energy in the middle of the target thickness, E^*_{CN} is the excitation energy of the compound nucleus (CN) calculated in the middle of the target, and I is the beam intensity. The last two columns represent the absolute time of measurements and evaluated production cross sections.

Fusion-evaporation reaction	E_{targ} (MeV)	E^*_{CN} (MeV)	I (pμA)	Time (h)	σ (nb)
^{207}Pb(^{50}Ti, 2n) ^{255}Rf	239.8	23.4	0.77	33.4	11.4 ± 1.8
^{208}Pb(^{50}Ti, 2n) ^{256}Rf	228.8	15.0	0.55	17.2	2.4 ± 0.3
	238.3	22.6	0.44	8.1	15.5 ± 1.7
^{209}Bi(^{50}Ti, 1n) ^{258}Db $\xrightarrow{\text{EC}}$ ^{258}Rf	232.6	16.0	0.63	195.6	2.9 ± 0.9

The selection rules for electromagnetic transitions require the multipolarity of the decay radiation at least as large as the change in the K value [7]. A large difference in K between initial and final state of a transition, hence a high transition multipolarity, results in a reduced transition probability, giving rise to metastable, long-lived states, so-called K isomers. The existence of K-isomeric states was previously reported in several even-even isotopes (e.g., ^{252}No [8], ^{254}No [9–11], ^{254}Rf [12], ^{256}Rf [13,14]), and odd-even or even-odd isotopes (e.g., ^{253}No [15,16], ^{255}Lr [17,18], ^{257}Rf [19]). In ^{255}Rf, only a single-particle $5/2^+[622]$ isomer with $T_{1/2} = 50 \pm 17\,\mu$s populated by α decay of ^{259}Sg was previously identified [6]. The population of isomeric state(s) with $T_{1/2} > 30\,\mu$s was recently confirmed also for direct production of ^{255}Rf [20]. One of the motivations of our work was therefore the search for K isomers in ^{255}Rf.

II. EXPERIMENT

Experiments aimed at the production of rutherfordium and dubnium ($Z = 105$) isotopes and investigations of their decay properties were carried out at GSI Darmstadt (Germany) using the velocity filter SHIP [21]. The beam of ^{50}Ti ions was accelerated by the UNILAC to energies from 225 to 243 MeV. The isotopes ^{255,256,258}Rf were produced in fusion-evaporation reactions ^{50}Ti + ^{207,208}Pb and ^{50}Ti + ^{209}Bi. Targets of ^{207}PbS, ^{208}PbS, and ^{209}Bi$_2$O$_3$ with thicknesses of 450, 450, and 463 μg/cm^2, respectively, were used. The evaporation residues (ERs) ^{255}Rf and ^{256}Rf were produced in the $2n$ evaporation channel while the ^{258}Rf was produced indirectly through the electron capture (EC) decay of ^{258}Db [22]. The irradiation details are summarized in Table I.

The ERs were separated from the primary beam by the velocity filter SHIP and delivered to the detection setup. After passing the time-of-flight system [23] they were implanted into a 16-strip position-sensitive silicon detector (STOP) placed at the focal plane of the separator. Six detectors (BOX) of the same type and shape arranged in a "box" geometry were mounted in front of the STOP detector to register escaping particles emitted into the backward hemisphere. A germanium clover detector (four crystals of 50–55 mm diameter and 70 mm length) was installed in close geometry behind the STOP detector for γ- and x-ray detection [24].

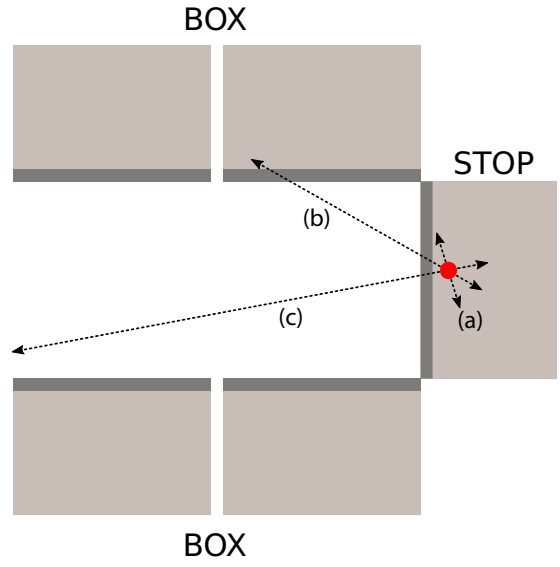

FIG. 1. Schematic view (not to scale) of STOP and BOX detectors registering fragments from SF of an implanted nucleus (side view with respect to the direction of implantation). The solid red circle represents an ER implanted into the STOP detector, while dotted-line arrows indicate the emission direction of the two fission fragments. The active area of the Si detectors is in light grey; dead layers are in dark grey. From the geometrical point of view, three possible cases can occur: (a) STOP-BOX anticoincidence (both fragments stay in STOP), (b) STOP-BOX coincidence (one fragment escapes to BOX), or (c) STOP-BOX anticoincidence (one completely escaped fragment). Note, scenarios (a) and (b) allow the reconstruction of the TKE, while (c) does not.

The implantation depth of ERs into the focal plane detector is typically a few micrometers while the range of fission fragments in silicon is 10–20 μm. When registering SF of ERs implanted in the STOP detector, three different situations can occur. Considering a 180° angle between the fission fragments, there is ≈60% probability (strongly depending on the ER implantation depth in the STOP detector) that both fragments are stopped in the STOP detector [Fig. 1(a)]. The remaining part includes events when one fragment escapes from the STOP detector in the backward direction. In this case there is an ≈80% probability for the escaping fragment to be detected by the BOX detector [denoted here as STOP-BOX coincidences; see Fig. 1(b)]. The remaining ≈20% of the escaping fragments are not detected [Fig. 1(c)]. Since fission events with one escaping fragment not registered by the BOX cannot be separated from the events with both fragments being stopped in the STOP detector, we refer to both cases as "STOP-BOX anticoincidences." For the cases with one fragment not detected, the fission energy cannot be fully reconstructed. The presence of these events in the spectrum results in a low-energy tail (for more details see Ref. [25]).

A. Correction of the energy deficit in TKE measurements

A crucial task for the evaluation of $\overline{\text{TKE}}$ using silicon detectors is the correction of the deficit in the measured energies.

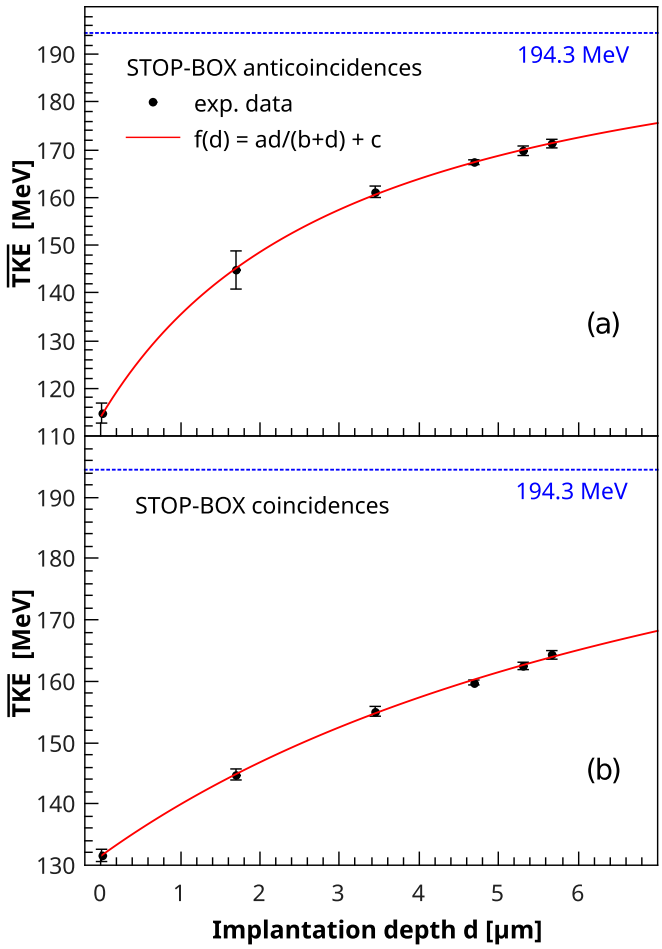

FIG. 2. $\overline{\text{TKE}}$ from the SF of ^{252}No as a function of implantation depth of ERs in the detector for (a) STOP-BOX anticoincident SF events and (b) STOP-BOX coincident SF events. Dashed blue line, $\overline{\text{TKE}} = 194.3$ MeV of ^{252}No from Ref. [29]; solid red line, saturation-growth fit of experimental data.

Two main effects influencing the TKE measurements were discussed in previous studies performed at SHIP [25–27].

First, the energy calibration of the silicon STOP and BOX detectors was based on α-decay energies of implanted nuclei. In contrast to signals from α particles, there is a pulse-height defect present for heavy ions including fission fragments (see, e.g., Ref. [28]), mainly caused by recombination of electron-hole pairs due the high local charge values created by the impact of the high-Z particle in the semiconductor. Second, there is a strong dependence of the energy deficit on the implantation depth into the STOP detector. Escaping fragments pass through the dead layers of STOP and BOX detectors under various angles, which leads to a larger loss of collected charges adding to the energy deficit.

To evaluate the energy deficit, we did a reanalysis of the data from Ref. [25], where the calibration reaction ^{48}Ca + ^{206}Pb was performed to produce ^{252}No for which a value of $\overline{\text{TKE}} = 194.3$ MeV is known from earlier work [29]. We measured the $\overline{\text{TKE}}$ of ^{252}No at six different implantation depths for STOP-BOX anticoincident [Fig. 2(a)] and coincident SF events [Fig. 2(b)]. Experimental values of $\overline{\text{TKE}}$ were fitted by a saturation-growth function (see Fig. 2). The calculation of energy loss of the ^{48}Ca projectiles in the target material (we assumed the reaction at half target thickness) as well as the energy loss of ^{252}No ERs in the target material, target backing foil, degrader foil, and implantation depths in the STOP detector were done using LISE++ [30]. The energy deficit at given implantation depth can then be determined as the energy difference of the known $\overline{\text{TKE}}$ of 194.3 MeV and the value from the fit curve of the experimental values as $\Delta E = (194.3 - \overline{\text{TKE}}_{\text{fit}})$ MeV.

Since the investigated rutherfordium isotopes are close in Z and A to ^{252}No, we applied the corrections evaluated above also here to correct the deficit in $\overline{\text{TKE}}$. The implantation depths of ERs were 6.5–6.8 μm. These depths correspond to energy corrections of 26–23 MeV for STOP-BOX coincidences and 22–19 MeV for anticoincidences. More details can be found in our previous report [31].

The full width at half maximum (FWHM) of TKE distribution for ^{252}No also changed as a function of the implantation depth. In the study of STOP-BOX coincidences we observed a slight decrease of FWHM from ≈38 MeV at 0.1 μm to ≈36 MeV at 5.4 μm.

B. Correction of the electron energies

For fast decays in our STOP detector (up to 500 μs) the decay signal [e.g., α decay or internal conversion electrons (CE)] is summed with the tail of ER signal. This pile-up effect causes a deviation of the measured decay energy which depends on the time difference between the ER implantation and the decay. For the investigation of electron energies in our work, discussed further in Sec. III E, it was necessary to determine an energy correction. We estimated this effect using the α decay of ^{216}Ac collected during the calibration measurement employing the reaction ^{50}Ti + ^{170}Er, which delivers a peak at 9118 keV in the α spectrum and has a half-life of 440 ± 16 μs. The plot of measured α-particle energy as a function of the time difference between the implantation and decay is shown in Fig. 3. A clear dependence can be seen, modifying the energy values of decays that occurred faster than 500 μs after the implantation of ER. We used the difference in measured and expected energies (green and red lines, respectively, in Fig. 3) at given times as an energy correction in our further analysis.

III. RESULTS

We registered several hundreds of SF events in each of the irradiations. To identify the SF events of ^{255}Rf and ^{256}Rf isotopes, we used the time and position correlation methods [32], based on delayed coincidences between the ER implantation and subsequent high-energy signal (corresponding to SF) in the same position of the detector. For ^{258}Rf we also searched for CEs after β decay of ^{258}Db produced in the reaction ^{50}Ti + ^{209}Bi and subsequent SF decay of the daughter nucleus ^{258}Rf. The searching time windows between either ER-SF or CE-SF correlations were set to about five times the half-life for each isotope. For the SF events, the energy condition window for high-energy signals was set to

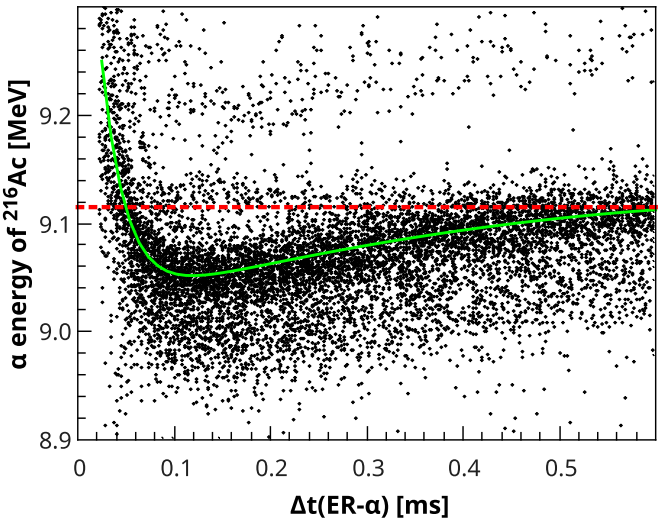

FIG. 3. Measured energy of the ^{216}Ac α decay as a function of the time after implantation of the ER. For fast decays, the α-decay signal is summed with the tail of the ER signal. The correction is given as the difference between the fitted measured energies (solid green line) and the nominal energy (dashed red line) at a given time.

100–300 MeV. Searching methods and conditions as well as the statistics of detected SF events for each isotope are described in Secs. III A–III C and summarized in Table II. We also searched for ER-CE-SF/α and ER-CE-CE-SF/α correlations in order to look for any possible isomers in ^{255}Rf. The details are described in Sec. III E.

A. ^{256}Rf produced in reaction ^{50}Ti + ^{208}Pb

The reaction ^{50}Ti + ^{208}Pb with the projectile energy set to 241.5 MeV (compound nucleus (CN) excitation energy of 22.6 MeV) was suited for the ^{256}Rf production through the 2n evaporation channel from the CN ^{258}Rf. For a part of the experiment the projectile energy was lowered to 232 MeV (CN excitation energy 15.0 MeV) to produce ^{257}Rf by the 1n evaporation channel. To detect the SF events, we searched for ER-SF correlations. The time-difference distribution of detected ER-SF events from this reaction is shown in Fig. 4(a). A time distribution corresponding to the half-life of ^{256}Rf ($T_{1/2} = 6.67$ ms [13]) was formed, well-separated from the distribution of random correlations without any visibly different SF activity.

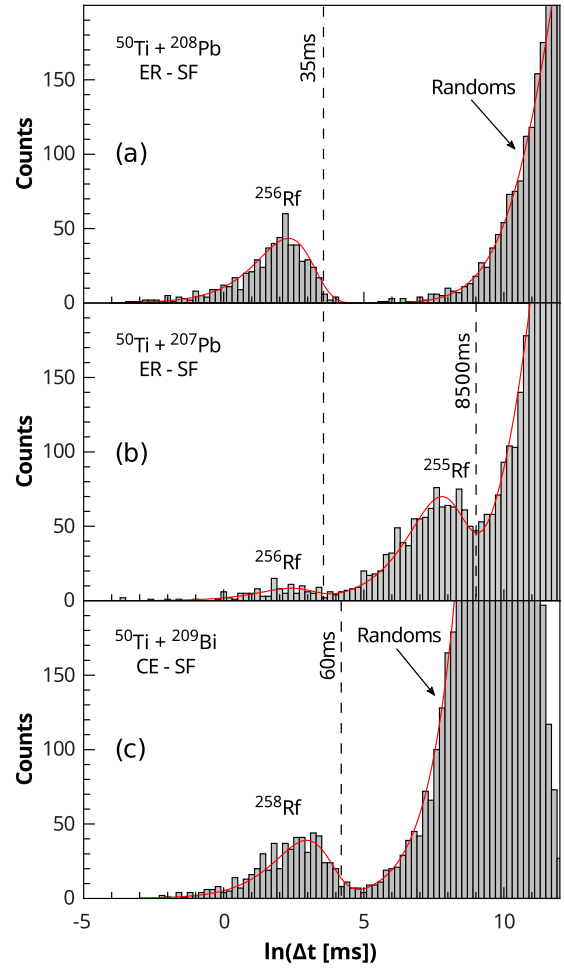

FIG. 4. Time-difference distributions obtained from the (a) ER-SF correlation search in the data from reaction ^{50}Ti + ^{208}Pb, (b) ER-SF correlation search in the data from reaction ^{50}Ti + ^{207}Pb, and (c) CE-SF correlation search in the data from reaction ^{50}Ti + ^{209}Bi. The dashed vertical lines represent the limits that were set for time-difference windows used to separate the isotopes: (a) 0–35 ms for ^{256}Rf, (b) 35–8500 ms for ^{255}Rf and (c) 0–60 ms for ^{258}Rf. Solid red lines represent the fit of the data with the universal function from the maximum likelihood method discussed in Ref. [33].

In total, we registered 591 SF events that were preceded by the implantation of ERs with time differences less than 35 ms. In 138 cases they were in coincidence with BOX detector

TABLE II. Statistics of SF events for each isotope from STOP-BOX coincident and anticoincident events. The searching time windows between either ER-SF or CE-SF were set to about five times the half-life for each isotope. For the SF events, the energy condition for high-energy signals was set to 100–300 MeV.

Isotope	Type of searched events	Condition	Counts (STOP-BOX coinc)	Counts (STOP-BOX anticoinc)
^{255}Rf	ER-SF	$\Delta t = 35$–8500 ms	160	715
^{256}Rf	ER-SF	$\Delta t = 0$–35 ms	138	453
^{258}Rf	SF	γ coinc	220	[a]
^{258}Rf	CE-SF	$\Delta t = 0$–60 ms	118	412

[a]In this case a coincidence with the BOX detector was required.

signals and the energy value was reconstructed summing the signals from STOP and BOX detectors.

We can exclude a possible SF contribution of ^{255}Rf at these beam energies. The number of ^{255}Rf fission events should be comparable to the α decays due to their similar branching values ($b_{SF} = 0.52 \pm 0.06$, $b_\alpha = 0.48 \pm 0.06$ [34]) and we did not observe any $\alpha(^{255}\text{Rf})$-$\alpha(^{251}\text{No})$ correlations ($b_\alpha(^{251}\text{No}) \approx 91\%$).

We also found about 700 ER-$\alpha(^{257}\text{Rf})$ correlations, mainly at the beam energy of 232 MeV. With respect to the branching ratio of 0.013 [35] for SF of ^{257}Rf and a half-life of 4.8 ± 0.2 s [36] the number of SF events for ^{257}Rf is negligible within $\Delta t = 35$ ms after the implantation of ERs.

We assigned all SF events detected during this reaction within the selected time window to ^{256}Rf. From the STOP-BOX coincident events, we evaluated a half-life of 6.75 ± 0.49 ms [see inset in Fig. 5(b)], which is in agreement with the half-life reported in Ref. [13].

B. ^{255}Rf produced in reaction ^{50}Ti + ^{207}Pb

The next case was the study of ^{255}Rf produced in the reaction $^{50}\text{Ti} + ^{207}\text{Pb}$ via the $2n$ evaporation channel from the CN ^{257}Rf. For this purpose, the beam energy was set to 243 MeV which corresponds to a CN excitation energy of 23.4 MeV.

Similarly to the reaction $^{50}\text{Ti} + ^{208}\text{Pb}$, discussed in the previous section, we also searched for ER-SF correlations. The time-difference distribution of detected ER-SF events is shown in Fig. 4(b). Two groups of events corresponding to SF activities of ^{256}Rf and ^{255}Rf were observed. For the identification of SF from ^{255}Rf we accepted only events with time differences between the ER and SF signals of 35–8500 ms. With regard to the time distribution for ^{256}Rf obtained in the reaction $^{50}\text{Ti} + ^{208}\text{Pb}$ [see Fig. 4(a)], the minimum time difference between ER and SF signals was set to 35 ms in order to avoid a contamination from ^{256}Rf (due to the $1n$ evaporation channel of the $^{50}\text{Ti} + ^{207}\text{Pb}$ reaction and possible ^{208}Pb impurities in the ^{207}Pb target resulting in $2n$ evaporation channel of the $^{50}\text{Ti} + ^{208}\text{Pb}$ reaction). The upper limit for the time window was set to 8500 ms, which is about five times the half-life of ^{255}Rf (1.68 ± 0.09 s reported in Ref. [37]).

In total, we identified 875 SF events corresponding to ^{255}Rf; 160 of them were in coincidence with the signal in the BOX detector. In about 20% of the cases, we found two possible ER candidates (ER_1 and ER_2) for one SF event within 35–8500 ms due to the fact that the end of the searching time window was already in the region of random correlations [see Fig. 4(b)]. Although this situation results in background for the time-difference distributions (both ER_1 and ER_2 are included), it does not effect the TKE distributions of SF events (each SF event is included only once). If ER_1 was in the range 0–35 ms before the SF event and ER_2 in 35–8500 ms, the assignment to ^{255}Rf or ^{256}Rf was questionable and we excluded this SF event from further TKE studies.

Among the events found within 35–8500 ms, we estimated the contribution of only three SF events that may originate from ^{256}Rf and, as there is no possibility for any other SF activity, we assigned all the events found within 35–8500 ms to ^{255}Rf and used these in the further TKE studies. From the STOP-BOX coincident events, we evaluated the half-life of 1.60 ± 0.07 s [see inset in Fig. 5(a)], which agrees with the half-life reported in Ref. [37].

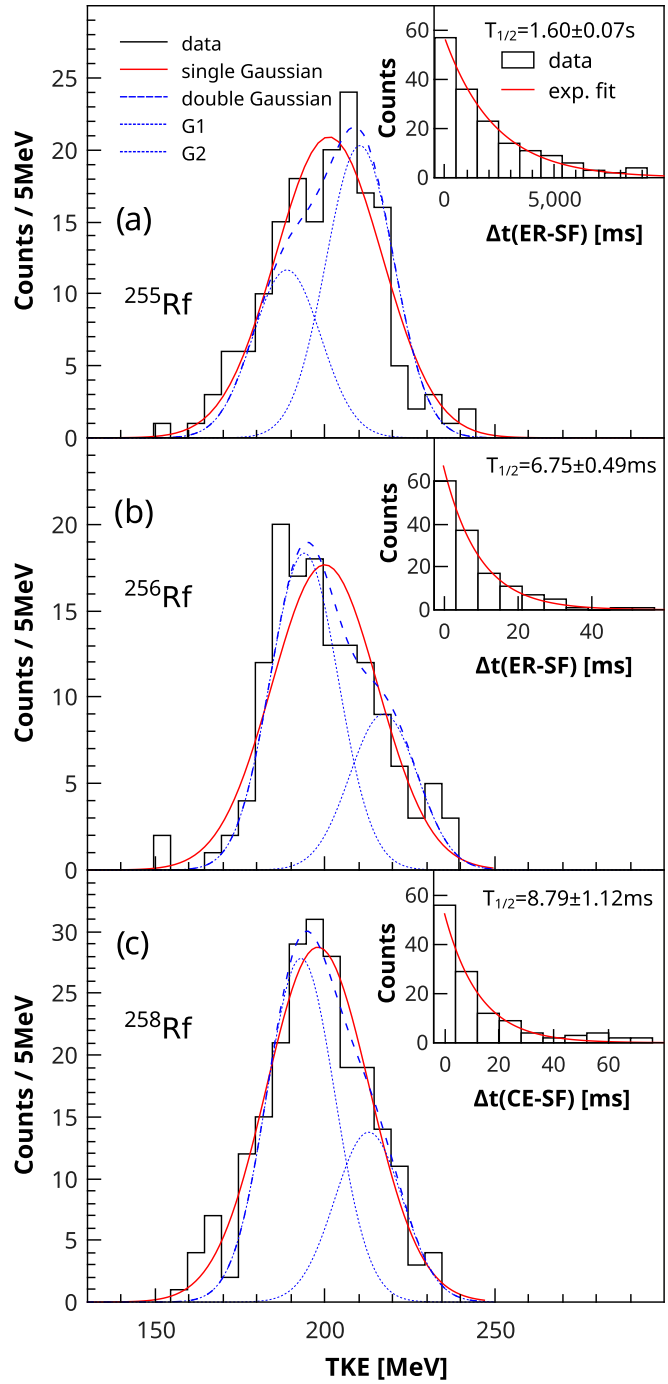

FIG. 5. TKE distributions of SF fragments from STOP-BOX coincidences (a) for SF of ^{255}Rf obtained from ER-SF correlations (inset shows ER-SF time differences), (b) for SF of ^{256}Rf obtained from ER-SF correlations (inset shows ER-SF time differences), and (c) for SF of ^{258}Rf obtained from STOP-BOX coincidences (inset shows CE-SF time differences in cases when CE was registered).

C. ^{258}Rf produced via EC decay of ^{258}Db

The reaction ^{50}Ti + ^{209}Bi with the projectile energy set to 236 MeV ($E^*_{CN} = 16.0$ MeV) was suited for the ^{258}Db production through the $1n$ evaporation channel. A considerable amount of ^{258}Rf was produced by EC decay of ^{258}Db ($b_{EC} = 0.23 \pm 0.08$ and $T_{1/2} = 4.3 \pm 0.5$ s reported in Ref. [11]). The investigations of the EC process in ^{258}Db and also α-decay studies of ^{258}Rf as well as the problems of ^{258}Rf SF identification in this case were reported in Refs. [22,38]. We searched for correlations between CE from the deexcitation of states in ^{258}Rf populated after the EC decay of ^{258}Db and subsequent SF. The time-difference distribution of detected CE-SF events is shown in Fig. 4(c).

We identified 530 SF events within a time window of 0–60 ms (about five times the half-life of ^{258}Rf) between CE and SF. In 118 cases, signals were in coincidence with the BOX detector. We assigned all events to ^{258}Rf. We used the CE-SF (STOP-BOX) time differences to determine a half-life of 8.79 ± 1.12 ms [see inset in Fig. 5(c)], which is in agreement with the values reported in Ref. [22].

However, we estimated that the detection efficiency for electrons was less than 50%. Thus, for further studies of STOP-BOX coincident events, we decided to take all high-energy events in coincidence with a signal from the clover detector (no correlation with CE) in order to increase the statistics in the TKE distribution. The high-energy background mainly comes from scattered projectiles that passed through the separator. The probability of STOP-BOX coincidences in the case of projectiles is very low. Only random coincidences can contribute. In addition, projectiles are not accompanied by γ rays as is the case for SF events. Thus, the criterion of a STOP-BOX-CLOVER coincidence is strongly selective for SF detection [25]. We found 220 of these events, which almost doubled the statistics in comparison with CE-SF correlations. Since there is no possible contribution from any other SF activity, we assigned all events to ^{258}Rf.

In the case of STOP-BOX anticoincident SF events, we still required correlations with CEs, since the criterion of a STOP-CLOVER coincidence is not as selective as a STOP-BOX-CLOVER coincidence, leaving a considerable amount of high-energy background events.

D. Total kinetic energies

To evaluate the TKE of SF events detected for each of the isotopes ^{255}Rf, ^{256}Rf, and ^{258}Rf, we used the correction method described in Sec. II A. The values of $\overline{\text{TKE}}$ obtained from all SF events (described in Fig. 1) for each isotope are summarized in Table III.

Then we separately treated only STOP-BOX coincident SF events with fully reconstructed energy [described in Fig. 1(b)]. The TKE distributions of STOP-BOX coincident events for ^{255}Rf, ^{256}Rf, and ^{258}Rf are shown in Fig. 5. We fitted the TKE distributions with single-Gaussian function and also with double-Gaussian function. For double-Gaussian fit we used a FWHM of 20 MeV for both Gaussian components as a fixed parameter (discussed in Sec. IV A). The $\overline{\text{TKE}}$ values, FWHM, and χ^2/degree of freedom (doF) values of single- and double-Gaussian fits for each isotope are summarized in Table IV.

TABLE III. Total kinetic energies evaluated in this work, compared to previous results. $\overline{\text{TKE}}_{\text{all}}$ was evaluated from all SF events obtained from both STOP-BOX coincidences and anticoincidences, $\overline{\text{TKE}}_{\text{ref}}$ is the reference value, and Ref. is the reference.

Isotope	$\overline{\text{TKE}}_{\text{all}}$ (MeV)	$\overline{\text{TKE}}_{\text{ref}}$ (MeV)	Ref.
^{255}Rf	199.5 ± 2.7	199 ± 3	[6]
^{256}Rf	198.7 ± 2.8	198.9 ± 4.4	[4]
^{258}Rf	198.2 ± 3.0	197.6 ± 1.1	[4]

By fitting with a single Gaussian we obtained $\overline{\text{TKE}}$ of 201.2 ± 0.9 MeV (FWHM $= 31.3 \pm 1.7$ MeV), 197.5 ± 1.0 MeV (FWHM $= 31.2 \pm 2.0$ MeV), and 197.9 ± 0.7 MeV (FWHM $= 30.3 \pm 1.4$ MeV) for the ^{255}Rf, ^{256}Rf, and ^{258}Rf isotopes, respectively.

By deconvolution with two Gaussian components we estimated the $\overline{\text{TKE}}$ of the low-energy and the high-energy components to be 186.3 ± 1.5 and 207.8 ± 0.8 MeV in the case of ^{255}Rf, 191.4 ± 0.7 and 214.8 ± 1.5 MeV in the case of ^{256}Rf, and 194.4 ± 1.5 and 213.5 ± 4.8 MeV in the case of ^{258}Rf.

E. Search for isomeric states in ^{255}Rf

To look for new possible isomeric states in ^{255}Rf we searched for correlations containing an electron signal from the deexcitation of an isomeric state by internal conversion, preceded by an ER signal and followed by a SF or α decay from the ground state (ER-CE-(CE)-SF/α). CEs were searched for in a time window of 500 μs after the ER implantation as a low-energy signal (up to 1 MeV). Subsequent α decays from the ground state (g.s.) of ^{255}Rf were searched for within 0–8500 ms and an energy range of 8500–9000 keV. For the SF, a time condition of 35–8500 ms was set in order to avoid a contamination from ^{256}Rf (with the same arguments that were mentioned in Sec. III B).

The detection system used in our study has some limitations for detection of low-energy electrons. For a significant part of the CEs the information on the position within the strip was missing. Therefore, we required a position agreement of the ER and SF/α signal to be within 1 mm and the same strip number for all three generations of a ER-CE-SF/α chain. We detected 144 ER-CE-SF/α correlations fulfilling the conditions mentioned above. The details are summarized in Table V.

In 74 cases the chains ended by SF and in 70 cases by α decay corresponding to ^{255}Rf and/or ^{251}No. The detection of ^{251}No α particles was preceded either by a full energy signal from the ^{255}Rf α decay or by 1–2 MeV signals originating from the escape of ^{255}Rf α particles from the detection system. We evaluated branching ratios of ^{255}Rf according to detector efficiencies to be $b_{SF} = 0.51 \pm 0.07$ and accordingly $b_\alpha = 0.49 \pm 0.07$. A contribution of a branching ratio for EC decay of ^{255}Rf (evaluated as < 0.06 in Ref. [6]) was not considered.

TABLE IV. In columns from left to right, for each isotope, characteristic values from fitting of TKE distributions (for SF events from STOP-BOX coincidences) are stated. For double-Gaussian fit: $\overline{\text{TKE}}_L$ of low-energy component, $\overline{\text{TKE}}_H$ of high-energy component, ΔE energy difference between $\overline{\text{TKE}}_L$ and $\overline{\text{TKE}}_H$, and the residual sum of squares (χ^2) divided by the degrees of freedom (doF). For single-Gaussian fit: $\overline{\text{TKE}}$, FWHM, and residual sum of squares (χ^2) divided by the degrees of freedom (doF). $\overline{\text{TKE}}_{\text{ref}}$ is the reference value and Ref. is the reference.

	Double-Gaussian fit				Single-Gaussian fit				
Isotope	$\overline{\text{TKE}}_L$ (MeV)	$\overline{\text{TKE}}_H$ (MeV)	ΔE (MeV)	χ^2/doF	$\overline{\text{TKE}}$ (MeV)	FWHM (MeV)	χ^2/doF	$\overline{\text{TKE}}_{\text{ref}}$ (MeV)	Ref.
^{255}Rf	186.3 ± 1.5	207.8 ± 0.8	21.8 ± 1.7	3.6	201.2 ± 0.9	31.3 ± 1.7	5.6	199 ± 3	[6]
^{256}Rf	191.4 ± 0.7	214.8 ± 1.5	23.4 ± 1.9	3.3	197.5 ± 1.0	31.2 ± 2.0	6.7	198.9 ± 4.4	[4]
^{258}Rf	194.4 ± 1.5	213.5 ± 4.8	19.1 ± 5.0	7.4	197.9 ± 0.7	30.3 ± 1.4	6.3	197.6 ± 1.1	[4]

In three cases of detected ER-CE-SF/α correlations, the CE was followed by another CE within 500 μs. The details on these three ER-CE-CE-SF/α(^{255}Rf) correlations including CE energies and decay times for each chain are summarized in Table VI.

From the total of 147 CEs detected in ER-CE-SF/α or ER-CE-CE-SF/α correlations, in 19 cases, CEs were in prompt coincidence with γ rays and in 128 cases without. The energy spectra of these CEs without or with coincident γ rays are shown in Figs. 6(a) and 6(b), respectively. The CE energies were corrected by the method discussed in Sec. II B. Figure 7 shows the two-dimensional (2D) plot of CE energies as a function of ER-CE time differences. The gap of $\approx$25 μs at the beginning is due to the dead time of the data acquisition system. We might separate the electrons into at least two groups according to their time distributions. The half-life of the lower-energy electrons (0–370 keV) is 35 ± 6 μs and of the higher-energy group (>370 keV) is 15^{+6}_{-4} μs.

We separately evaluated the half-life of the lower-energy CEs (0–370 keV) in coincidence with γ rays as 38^{+12}_{-7} μs (explained in the discussion in Sec. IV B). The energy spectra of coincident γ rays are shown in Fig. 8. There is no sign of any distinct γ lines in single-crystal mode or add-back mode of the clover detector. The spectrum of summed energies of electrons and coincident γ rays is shown in Fig. 6(c), where energies go up to 1050 keV.

IV. DISCUSSION

A. Total kinetic energies

As was mentioned in Sec. II the spectra from STOP-BOX anticoincidences contain a small part of events where one of the fragments escaped without being detected in the BOX detector. These events have incomplete energy and affect the shape of the TKE distribution (see discussion in Ref. [25]). These distributions are therefore not suitable for the analysis of their shape, as would be desirable for the search of bimodal fission; however, they could still be scaled to allow an evaluation of $\overline{\text{TKE}}$. The $\overline{\text{TKE}}$ of ^{255}Rf SF is 199.5 ± 2.7 MeV, which is in a good agreement with the value of 199 ± 3 MeV from Ref. [6], where ^{255}Rf was produced at SHIP indirectly by α decay of ^{259}Sg and the method from Ref. [27] was used to correct $\overline{\text{TKE}}$ for the energy deficit. The $\overline{\text{TKE}}$ values of 198.7 ± 2.8 MeV for ^{256}Rf and 198.2 ± 3.0 MeV for ^{258}Rf are also in a good agreement with previously measured 198.9 ± 4.4 MeV and 197.6 ± 1.1 MeV [4], respectively. The TKE distributions containing all types of SF events have a FWHM $\approx$37 MeV for all three isotopes.

To study the shape of TKE distributions, it is necessary to use only STOP-BOX coincident events with completely registered energy as a sum of energies from STOP and BOX detectors. From the results of single-Gaussian fitting of the TKE distributions we can state that for all three isotopes ^{255}Rf, ^{256}Rf, and ^{258}Rf we observed TKE distributions that were more narrow (30–31 MeV) than in the case of ^{252}No from the calibration reaction (36–38 MeV) discussed in Sec. II A, and also than the reported cases of bimodal fission in ^{258}Fm, ^{259,260}Md, and ^{258,262}No. $\overline{\text{TKE}}$ of the distributions for ^{255}Rf, ^{256}Rf, and ^{258}Rf were $\approx$200 MeV. Similar values for $\overline{\text{TKE}}$ were obtained in previous studies for the TKE distribution of ^{258}Rf [4] and ^{260}Rf [5]. The $\overline{\text{TKE}}$ value of $\approx$200 MeV also corresponds with the value for the lower-energy fission mode in reported cases of bimodal fission for isotopes ^{258}Fm, ^{259,260}Md, and ^{258,262}No [5]. We did not observe any SF events for ^{255}Rf, ^{256}Rf, and ^{258}Rf with TKE $\approx$233 MeV, that would correspond to the $\overline{\text{TKE}}$ of a higher-energy fission mode as it was observed in reported bimodal-fission cases.

The distribution for the isotope ^{258}Rf is rather symmetric. A slight asymmetry in the TKE distributions of ^{255}Rf and ^{256}Rf is noticeable. In this case one cannot exclude the

TABLE V. Summary of ER-CE-SF/α correlation search. The time and energy conditions are stated. In 74 cases, chains ended by SF; in 70 cases by α decay of ^{255}Rf or ^{251}No.

Correlation	Δt(ER-CE) range	Δt(CE-SF/α) range	E range	Counts
ER-CE-(CE)-SF(^{255}Rf)	500 μs	35–8500 ms	100–300 MeV	74
ER-CE-(CE)-α(^{255}Rf)-(α(^{251}No))	500 μs	0–8500 ms	8500–9000 keV	70

TABLE VI. CE characteristics from the ER-CE-CE-SF/α correlations.

ER-CE-CE-SF/α chain	E_{CE1} (keV)	Δt_{CE1} (μs)	E_{CE2} (keV)	Δt_{CE2} (μs)	g.s. decay
1	81.0	57	147.5	33	SF
2	126.0	88	143.8	25	α
3	146.4	50	19.8[a]	26	α

[a]The second electron from the third chain was in coincidence with 305.6-keV γ ray.

possibility of bimodal fission in these isotopes, as it was predicted by theoretical calculations [3], although in this case, the two possible fission modes would have $\overline{\text{TKE}}$ closer than in known cases in ^{258}Fm, ^{259,260}Md, and ^{258,262}No. For this purpose we also provided a fit of the TKE distributions by double-Gaussian function.

During the fitting procedure we used the value of 20 MeV as a fixed width for both Gaussian components. The TKE distributions for all three isotopes were themselves 30–31 MeV wide and we could not use any FWHM value obtained from other isotopes, generally considered as single-mode fissioning (e.g., ^{252}No) as a reference value during the fitting since the FWHM of ^{252}No was 36–38 MeV.

The quality of single- or double-Gaussian fits can be characterized by the values of the residual sum of squares (χ^2) divided by the degrees of freedom (doF). The values of χ^2/doF are suitable for comparison only for histograms with similar statistics (considering the same binning). Thus, the quality of single- or double-Gaussian fits for TKE distributions can be compared via χ^2/doF only for the same isotope. For ^{255}Rf, χ^2/doF was lower in the case of the double-Gaussian as compared with the single-Gaussian fit. For ^{256}Rf the situation was the same. In the case of ^{258}Rf, the χ^2/doF value for the double-Gaussian fit was higher.

Asymmetric TKE distributions and lower χ^2/doF values for double-Gaussian fits lead us to the conclusion of possible bimodal fission for ^{255}Rf and ^{256}Rf. For ^{255}Rf the high-energy component is dominant while for ^{256}Rf the low-energy component is dominant. In ^{258}Rf we do not clearly see asymmetry in the TKE distribution and the double-Gaussian fit gives a slightly higher χ^2/doF value than the single-Gaussian fit, which means that this isotope is either fissioning by only one fission mode or there are two fission modes with similar abundances, adding up to a symmetric TKE distribution. Such a possibility for ^{258}Rf also resulted from the theoretical calculations [3].

From the fact mentioned above we can summarize that in any of the three isotopes ^{255}Rf, ^{256}Rf, and ^{258}Rf we did not observe TKE distributions that would confirm the presence of two fission modes at ≈200 and ≈233 MeV as it was common for all four, up-to-now reported cases of bimodal fission in ^{258}Fm, ^{259,260}Md, and ^{258,262}No [4,5]. However, the bimodal fission for ^{256}Rf and ^{258}Rf was predicted by theoretical calculations and the experimental TKE distributions are in qualitative agreement: asymmetric for ^{256}Rf with dominant lower-energy mode and symmetric for ^{258}Rf. In the cases of ^{255}Rf and ^{256}Rf the idea of bimodal fission

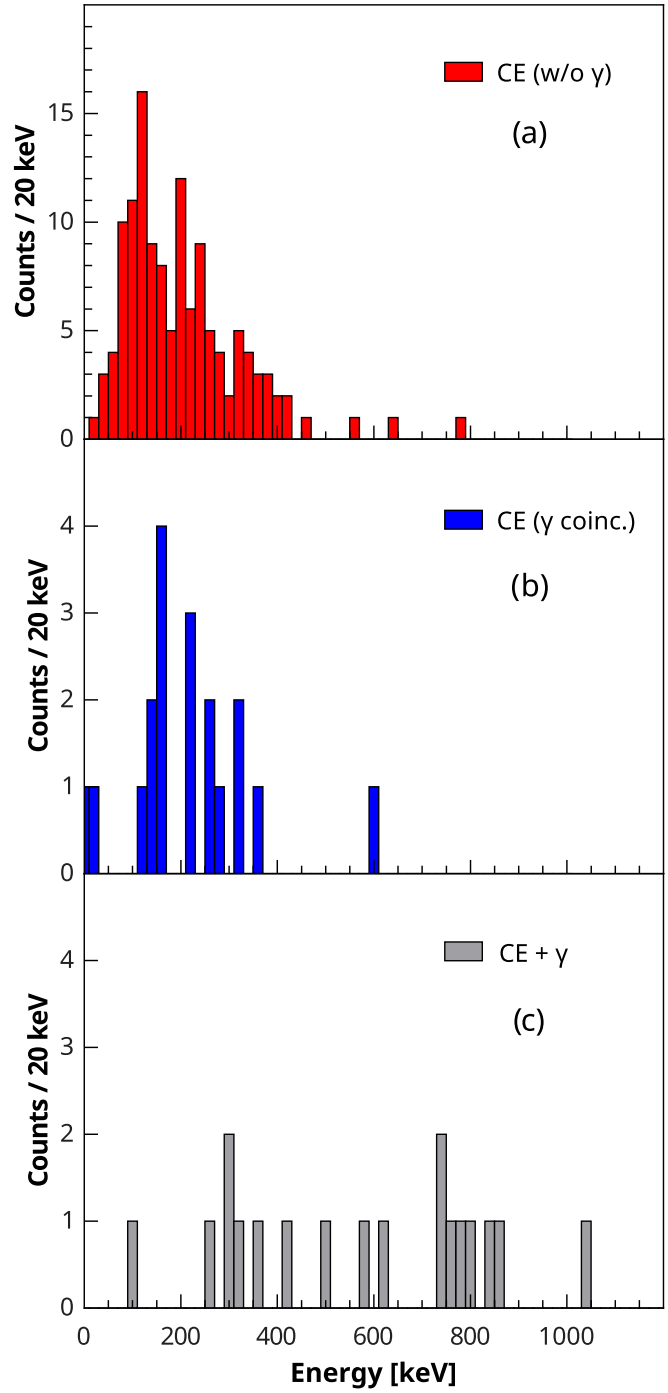

FIG. 6. Energies of conversion electrons from the ER-CE-(CE)-SF/α correlations: (a) electrons not coincident with γ rays, (b) electrons in coincidence with γ rays, and (c) summed energies of electrons and coincident γ rays.

is supported (besides the asymmetric TKE distributions) by lower χ^2/doF values for double-Gaussian fits than single-Gaussian fits. If there is a bimodal fission present in ^{255}Rf, ^{256}Rf, or ^{258}Rf, it has completely different characteristics than cases reported in Fm–No isotopes—the components of ≈20 MeV FWHM are closer to each other at energies of ≈190 and ≈210 MeV.

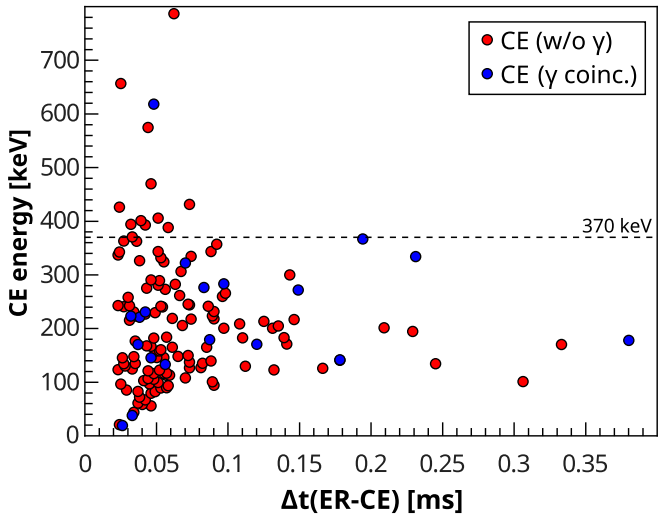

FIG. 7. CE energies as a function of the time difference between the implantation of an ER and the detection of a CE. Red dots, electrons not in coincidence with γ rays; blue dots, electrons in coincidence with γ rays.

B. *K* isomers in ^{255}Rf

The previously identified single-particle $5/2^+[622]$ isomer in ^{255}Rf (populated by α decay of ^{259}Sg) with $T_{1/2} = 50 \pm 17\,\mu$s at excitation energy of ≈135 keV [6] was based on the statistics of 42 ER(^{259}Sg)-α-CE correlations. None of the CEs in the previous study was observed in coincidence with γ rays. The energy distribution of the electrons formed a narrow peak at ≈105 keV with FWHM practically defined only by detector resolution.

The $5/2^+[622]$ isomers in the $N = 151$ isotones essentially decay by $M2$ transitions (with some $E3$ contributions) into the $9/2^-[734]$ ground state (see studies of ^{255}No $\xrightarrow{\alpha}$ ^{251}Fm [39] and ^{257}Rf $\xrightarrow{\alpha}$ ^{253}No [22]). These transitions are predominantly K-converted, as seen from α-decay studies and also from direct population (as for ^{253}No). These $5/2^+[622] \rightarrow 9/2^-[734]$ transitions were identified by α-x-ray/γ or ER-x-ray/γ coincidences without coincident CE. In the α-decay study of ^{259}Sg no delayed coincidences between ^{259}Sg α decays and K-x-rays were observed, proving that the excitation energy of the $5/2^+[622]$ isomer must be below the K-binding energy (i.e., ≈160 keV); the CEs presented in the ^{259}Sg study thus stem from L conversion. This, however, means that within decay of the $5/2^+[622]$ isomer no CEs at $E > 160$ keV can significantly be observed.

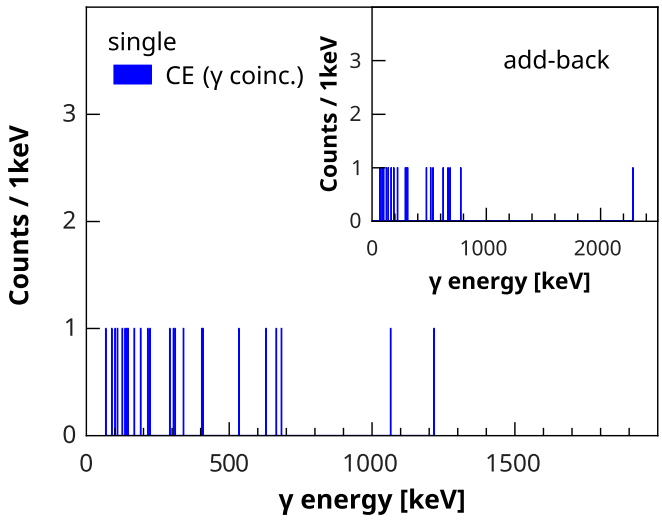

FIG. 8. Energy spectrum of γ rays in coincidence with electrons from the ER-CE-(CE)-SF/α correlations. Inset: add-back spectrum.

In our study, with direct production of ^{255}Rf via the $2n$ evaporation channel, the results are different from those reported for the $5/2^+[622]$ single-particle isomer. The energy distribution of 147 CEs we detected in ER-CE-(CE)-α/SF correlations was significantly broader and reaching up to 800 keV [see Fig. 6(a)]. Also 19 CEs were detected in coincidence with γ rays. Since CEs with energies above ≈200 keV cannot originate in the decay of the $5/2^+[622]$ isomer, the observation of higher-energy CEs in our data indicates the presence of new isomer(s) in ^{255}Rf.

From Fig. 7 it seems that CEs that were detected with higher energies ($\gtrsim$370 keV) have a shorter half-life than CEs with lower energies. Therefore, we divided CEs in two subsets according to their energies and treated them separately. The limit of 370 keV was based on the CE with the highest energy from the lower-energy group with significantly longer lifetimes.

In the energy range 0–370 keV, we found that most of the CEs were not in coincidence with γ rays. The half-life of these events was $35 \pm 6\,\mu$s. The fact that many electrons were not in coincidence with γ rays can be explained by the γ-ray detection efficiency; however, we cannot exclude a contribution from the $5/2^+[622]$ isomer with $T_{1/2} = 50 \pm 17\,\mu$s half-life, for which no γ rays were observed in coincidence with CEs [6]. As these events result in similar half-lives and energies, they cannot be separated from the electrons originating in the deexcitation of the new isomer we identified. However, in 18 cases, lower-energy CEs were detected in coincidence with γ rays. Thus, we based the estimations of new isomer properties on these events, as they cannot originate in the known $5/2^+[622]$ isomer. These events led to the value for a half-life of $38^{+12}_{-7}\,\mu$s.

From the high number of electrons in comparison with the number of γ rays and nonobservation of a clear γ-ray peak, we assume that the transition deexciting the isomer has a high total conversion coefficient. However, for low-multipolarity transitions high conversion coefficients are expected only for low transition energies up to 100–200 keV. Therefore, we consider our electron signals to be formed as a summed signal from a cascade of three to five transitions. The ground state of ^{255}Rf was assigned to be the $9/2^-[734]$ state in Ref. [37] and thus the new isomer should be a high-K isomer with a K number at least by 4–6 higher than the ground state. The excitation energy can be estimated from the summed energies of conversion electrons and coincident γ rays [Fig. 6(c)], which go up to 1050 keV. Depending on the binding energies of electrons in the atomic K (≈147 keV) or L (≈29 keV) shells, the excitation energy is roughly estimated to 1150–1450 keV.

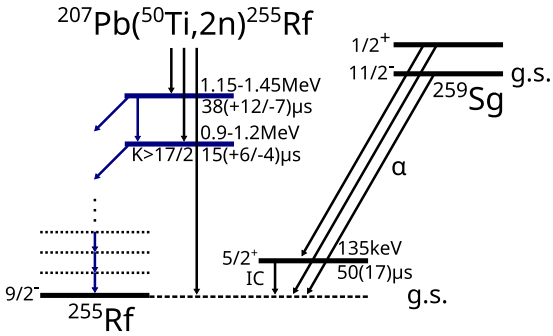

FIG. 9. Proposed decay scheme of the K isomers in ^{255}Rf, populated in the reaction ^{207}Pb(^{50}Ti, $2n$) ^{255}Rf (left) and in the α decay of ^{259}Sg (right).

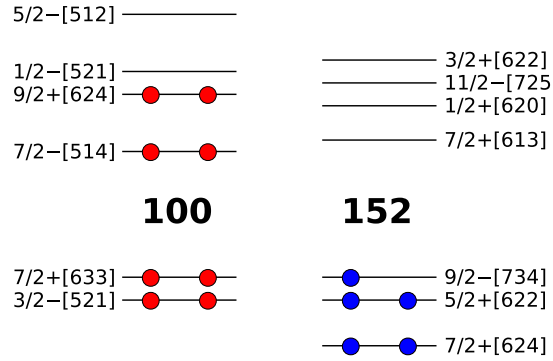

FIG. 10. Single-particle levels for protons (left) and neutrons (right) in ^{255}Rf, calculated in Ref. [40] with nuclear deformations taken from Ref. [41]. The neutron level $5/2^+[622]$ was placed according to experimental results from Ref. [6]. The ground-state configuration is shown.

At higher energies (>370 keV), another group of 13 CEs (one of them in coincidence with γ ray) with significantly shorter lifetime than lower-energy CEs (assigned above to a new isomer) was formed (Fig. 7). The half-life of these events is 15^{+6}_{-4} μs. Using the same arguments as above one can expect these signals to be the sum of an electron cascade from the deexcitation of another high-K isomeric state with significantly shorter half-life. As the energies of electrons with $T_{1/2} = 15^{+6}_{-4}$ μs reach up to 800 keV one can estimate the excitation energy to be 900–1200 keV.

A supporting argument for an existence of two isomers is also the observation of three ER-CE-CE-SF/α(^{255}Rf) correlations shown in Table VI. We estimated that the total amount of random correlations of this type in our measurement is below 2×10^{-6}. In all three cases, the decay time of the first electron was significantly longer than the decay time of the second one. From this fact we assume that besides a direct population of the 15-μs isomer during the production of the ER, the decay of the longer-lived 38-μs isomer might also feed the 15-μs isomer. Considering only the decay times and energies of the second electrons in the chains, one also cannot exclude the possibility of population of the $5/2^+[622]$ isomer. However, given the fact that the second electron from the third chain was in coincidence with a γ ray which should not be present for $5/2^+[622]$ deexcitation, this scenario seems to be less likely.

The order and energy gap between two new isomeric states can be estimated from the energies of the first CEs from ER-CE-CE-SF/α(^{255}Rf) correlations. By adding the binding energy of an electron on the K or L atomic shell we estimated the gap between the two isomeric levels to be 150–300 keV. Based on the results presented before we propose the tentative decay scheme shown in Fig. 9.

The crucial question for such an interpretation is the availability of levels to form a configuration with a high K value. The scheme of available single-particle levels for protons and neutrons in ^{255}Rf prepared according to calculations from Ref. [40] with nuclear deformations taken from Ref. [41] is presented in Fig. 10. The order and also energy gaps between proton and neutron single-particle levels should be understood as rather illustrative and may vary for different calculations. In the case of ^{255}Rf a high-K configuration can be simply achieved for example by breaking a pair of protons at $9/2^+[624]$ and shifting one proton to the $1/2^-[521]$ level. Such a three-quasiparticle configuration $\{1/2^-[521]\pi \otimes 9/2^+[624]\pi \otimes 9/2^-[734]\nu\}$ leads to $K = 19/2^+$ with $\Delta K = 5$. However, many different configurations are possible. The calculated configurations of 2-qp isomer in the neighboring isotopes ^{254}Rf and ^{256}Rf reported in Refs. [12,19] should be considered as well in ^{255}Rf with an additional unpaired neutron. The 3-qp configurations composed of three unpaired neutrons demand a neutron to be lifted over the level gap for deformed isotones at $N = 152$. From the estimations of the excitation energy of the new isomers, a quite low-lying high-K state can be expected. Nevertheless, without having detailed calculations of energy gaps, one cannot exclude the possibility of a three-neutron qp state.

V. CONCLUSION

The correction of the energy deficit in TKE studied for ^{252}No allowed us to evaluate the $\overline{\text{TKE}}$ of the rutherfordium isotopes ^{255}Rf, ^{256}Rf, and ^{258}Rf to be 199.5 ± 2.7, 198.7 ± 2.8, and 198.2 ± 3.0 MeV, respectively. The results on $\overline{\text{TKE}}$ are in good agreement with previous studies. To investigate the TKE distributions, we considered only STOP-BOX coincident events with fully reconstructed energy. The TKE distributions were positioned around 200 MeV with FWHM of 30–31 MeV. We did not observe the TKE distributions with two energy components at ≈200 and ≈233 MeV as it was in reported cases of bimodal fission in ^{258}Fm, ^{259,260}Md, and ^{258,262}No. However, we observed asymmetric distributions for ^{255}Rf and ^{256}Rf and a more symmetric shape for ^{258}Rf. A possible explanation is the existence of bimodal fission for ^{255}Rf and ^{256}Rf, although with different characteristics as in previous cases. Double-Gaussian fitting deconvolution leads to closer $\overline{\text{TKE}}$ values of ≈190 and ≈210 MeV.

In the study of CEs detected in ER-CE-CE-SF/α(^{255}Rf) correlations, we identified two new high-K, presumably 3-qp, isomers in ^{255}Rf with half-lives of $T_{1/2} = 38^{+12}_{-7}$ μs and $T_{1/2} = 15^{+6}_{-4}$ μs. Estimated excitation energies of these

isomers are 1150–1450 and 900–1200 keV, respectively, with 150–300 keV of energy difference between them and a lower limit for spin of $17/2\hbar$.

ACKNOWLEDGMENTS

We thank the UNILAC staff as well as the ion source crew for delivering beams of high and stable intensity. We are also grateful to J. Steiner for production of the large area targets. We want to express our gratitude to H. G. Burkhard and J. Maurer for skillful maintenance of the mechanical and electrical components of SHIP and A. Bronis for help during the analysis. Three of us, B.A., S.A., and P.M., were supported by the Slovak Research and Development Agency (Contract No. APVV-14-0524) and by the Slovak grant agency VEGA (Contract No. 1/0532/17).

[1] S. G. Nilsson, C. F. Tsang, A. Sobiczewski, Z. Szymanski, S. Wycech, C. Gustafson, I.-L. Lamm, P. Möller, and B. Nilsson, Nucl. Phys. A **131**, 1 (1969).
[2] F. P. Heßberger, Eur. Phys. J. A **53**, 75 (2017).
[3] N. Carjan, F. A. Ivanyuk, Y. Oganessian, and G. Ter-Akopian, Nucl. Phys. A **942**, 97 (2015).
[4] J. F. Wild, E. K. Hulet, R. W. Lougheed, K. J. Moody, B. B. Bandong, R. J. Dougan, and A. Veeck, J. Alloys Compd. **213**, 86 (1994).
[5] E. K. Hulet, J. F. Wild, R. J. Dougan, R. W. Lougheed, J. H. Landrum, A. D. Dougan, P. A. Baisden, C. M. Henderson, R. J. Dupzyk, R. L. Hahn, M. Schädel, K. Sümmerer, and G. R. Bethune, Phys. Rev. C **40**, 770 (1989).
[6] S. Antalic, F. P. Heßberger, D. Ackermann, S. Heinz, S. Hofmann, B. Kindler, J. Khuyagbaatar, B. Lommel, and R. Mann, Eur. Phys. J. A **51**, 41 (2015).
[7] K. Löbner, Phys. Lett. B **26**, 369 (1968).
[8] B. Sulignano, S. Heinz, F. P. Heßberger, S. Hofmann, D. Ackermann, S. Antalic, B. Kindler, I. Kojouharov, P. Kuusiniemi, B. Lommel, R. Mann, K. Nishio, A. G. Popeko, S. Saro, B. Streicher, M. Venhart, and A. V. Yeremin, Eur. Phys. J. A **33**, 327 (2007).
[9] A. Ghiorso, K. Eskola, P. Eskola, and M. Nurmia, Phys. Rev. C **7**, 2032 (1973).
[10] R.-D. Herzberg, P. T. Greenlees, P. A. Butler, G. D. Jones, M. Venhart, I. Darby, S. Eeckhaudt, K. Eskola, T. Grahn, C. Gray-Jones, F. P. Hessberger, P. Jones, R. Julin, S. Juutinen, S. Ketelhut, W. Korten, M. Leino, A.-P. Leppänen, S. Moon, and J. Uusitalo, Nature (London) **442**, 896 (2006).
[11] F. P. Heßberger, S. Antalic, B. Sulignano, D. Ackermann, S. Heinz, S. Hofmann, B. Kindler, J. Khuyagbaatar, I. Kojouharov, P. Kuusiniemi, M. Leino, B. Lommel, R. Mann, K. Nishio, A. G. Popeko, Š. Šáro, B. Streicher, J. Uusitalo, M. Venhart, and A. V. Yeremin, Eur. Phys. J. A **43**, 55 (2009).
[12] H. M. David, J. Chen, D. Seweryniak, F. G. Kondev, J. M. Gates, K. E. Gregorich, I. Ahmad, M. Albers, M. Alcorta, B. B. Back, B. Baartman, P. F. Bertone, L. A. Bernstein, C. M. Campbell, M. P. Carpenter, C. J. Chiara, R. M. Clark, M. Cromaz, D. T. Doherty, G. D. Dracoulis, N. E. Esker, P. Fallon, O. R. Gothe, J. P. Greene, P. T. Greenlees, D. J. Hartley, K. Hauschild, C. R. Hoffman, S. S. Hota, R. V. F. Janssens, T. L. Khoo, J. Konki, J. T. Kwarsick, T. Lauritsen, A. O. Macchiavelli, P. R. Mudder, C. Nair, Y. Qiu, J. Rissanen, A. M. Rogers, P. Ruotsalainen, G. Savard, S. Stolze, A. Wiens, and S. Zhu, Phys. Rev. Lett. **115**, 132502 (2015).
[13] H. B. Jeppesen, I. Dragojević, R. M. Clark, K. E. Gregorich, M. N. Ali, J. M. Allmond, C. W. Beausang, D. L. Bleuel, M. Cromaz, M. A. Deleplanque, P. A. Ellison, P. Fallon, M. A. Garcia, J. M. Gates, J. P. Greene, S. Gros, I. Y. Lee, H. L. Liu, A. O. Macchiavelli, S. L. Nelson, H. Nitsche, J. R. Pavan, L. Stavsetra, F. S. Stephens, M. Wiedeking, R. Wyss, and F. R. Xu, Phys. Rev. C **79**, 031303(R) (2009).
[14] A. P. Robinson, T. L. Khoo, D. Seweryniak, I. Ahmad, M. Asai, B. B. Back, M. P. Carpenter, P. Chowdhury, C. N. Davids, J. Greene, P. T. Greenlees, K. Hauschild, A. Heinz, R.-D. Herzberg, R. V. F. Janssens, D. G. Jenkins, G. D. Jones, S. Ketelhut, F. G. Kondev, T. Lauritsen, C. J. Lister, A. Lopez-Martens, P. Marley, E. McCutchan, P. Papadakis, D. Peterson, J. Qian, D. Rostron, U. Shirwadkar, I. Stefanescu, S. K. Tandel, X. Wang, and S. Zhu, Phys. Rev. C **83**, 064311 (2011).
[15] A. Lopez-Martens, K. Hauschild, A. V. Yeremin, O. Dorvaux, A. V. Belozerov, C. Briançon, M. L. Chelnokov, V. I. Chepigin, D. Curien, P. Désesquelles, B. Gall, V. A. Gorshkov, M. Guttormsen, F. Hanappe, A. P. Kabachenko, F. Khalfallah, A. Korichi, A. C. Larsen, O. N. Malyshev, A. Minkova, Y. T. Oganessian, A. G. Popeko, M. Rousseau, N. Rowley, R. N. Sagaidak, S. Sharo, A. V. Shutov, S. Siem, L. Stuttgé, A. I. Svirikhin, N. U. H. Syed, and C. Theisen, Eur. Phys. J. A **32**, 245 (2007).
[16] S. Antalic, F. P. Heßberger, D. Ackermann, S. Heinz, S. Hofmann, Z. Kalaninová, B. Kindler, J. Khuyagbaatar, I. Kojouharov, P. Kuusiniemi, M. Leino, B. Lommel, R. Mann, K. Nishio, Š. Šáro, B. Streicher, B. Sulignano, and M. Venhart, Eur. Phys. J. A **47**, 62 (2011).
[17] S. Antalic, F. P. Heßberger, S. Hofmann, D. Ackermann, S. Heinz, B. Kindler, I. Kojouharov, P. Kuusiniemi, M. Leino, B. Lommel, R. Mann, K. Nishio, Š. Šáro, B. Streicher, B. Sulignano, and M. Venhart, Eur. Phys. J. A **38**, 219 (2008).
[18] K. Hauschild, A. Lopez-Martens, A. V. Yeremin, O. Dorvaux, S. Antalic, A. V. Belozerov, C. Briançon, M. L. Chelnokov, V. I. Chepigin, D. Curien, B. Gall, A. Görgen, V. A. Gorshkov, M. Guttormsen, F. Hanappe, A. P. Kabachenko, F. Khalfallah, A. C. Larsen, O. N. Malyshev, A. Minkova, A. G. Popeko, M. Rousseau, N. Rowley, S. Saro, A. V. Shutov, S. Siem, L. Stuttgè, A. I. Svirikhin, N. U. H. Syed, C. Theisen, and M. Venhart, Phys. Rev. C **78**, 021302(R) (2008).
[19] J. Rissanen, R. M. Clark, K. E. Gregorich, J. M. Gates, C. M. Campbell, H. L. Crawford, M. Cromaz, N. E. Esker, P. Fallon, U. Forsberg, O. Gothe, I.-Y. Lee, H. L. Liu, A. O. Machiavelli, P. Mudder, H. Nitsche, G. Pang, A. Rice, D. Rudolph, M. A. Stoyer, A. Wiens, and F. R. Xu, Phys. Rev. C **88**, 044313 (2013).
[20] J. Khuyagbaatar, A. Mistry, D. Ackermann, L.-L. Andersson, M. Block, H. Brand, C. Düllmann, J. Even, F. Heßberger, J. Hoffmann, A. Hübner, E. Jäger, B. Kindler, J. Krier, N. Kurz, B. Lommel, B. Schausten, J. Steiner, A. Yakushev, and V. Yakusheva, Nucl. Phys. A **994**, 121662 (2020).

[21] G. Münzenberg, W. Faust, S. Hofmann, P. Armbruster, K. Güttner, and H. Ewald, Nucl. Instrum. Methods **161**, 65 (1979).
[22] F. P. Heßberger, S. Antalic, D. Ackermann, B. Andel, M. Block, Z. Kalaninova, B. Kindler, I. Kojouharov, M. Laatiaoui, B. Lommel, A. K. Mistry, J. Piot, and M. Vostinar, Eur. Phys. J. A **52**, 328 (2016).
[23] Š. Šáro, R. Janik, S. Hofmann, H. Folger, F. Heßberger, V. Ninov, H. Schött, A. Kabachenko, A. Popeko, and A. Yeremin, Nucl. Instrum. Methods Phys. Res., Sect. A **381**, 520 (1996).
[24] S. Hofmann and G. Münzenberg, Rev. Mod. Phys. **72**, 733 (2000).
[25] S. Hofmann, D. Ackermann, S. Antalic, H. G. Burkhard, V. F. Comas, R. Dressler, Z. Gan, S. Heinz, J. A. Heredia, F. P. Heßberger, J. Khuyagbaatar, B. Kindler, I. Kojouharov, P. Kuusiniemi, M. Leino, B. Lommel, R. Mann, G. Münzenberg, K. Nishio, A. G. Popeko, S. Saro, H. J. Schött, B. Streicher, B. Sulignano, J. Uusitalo, M. Venhart, and A. V. Yeremin, Eur. Phys. J. A **32**, 251 (2007).
[26] F. P. Heßberger, G. Münzenberg, S. Hofmann, Y. K. Agarwal, K. Poppensieker, W. Reisdorf, K. H. Schmidt, J. R. H. Schneider, W. F. W. Schneider, H. J. Schött, P. Armbruster, B. Thuma, C. C. Sahm, and D. Vermeulen, Z. Phys. A **322**, 557 (1985).
[27] K. Nishio, S. Hofmann, F. P. Heßberger, D. Ackermann, S. Antalic, V. F. Comas, Z. Gan, S. Heinz, J. A. Heredia, H. Ikezoe, J. Khuyagbaatar, B. Kindler, I. Kojouharov, P. Kuusiniemi, B. Lommel, M. Mazzocco, S. Mitsuoka, Y. Nagame, T. Ohtsuki, A. G. Popeko, S. Saro, H. J. Schött, B. Sulignano, A. Svirikhin, K. Tsukada, K. Tsuruta, and A. V. Yeremin, AIP Conf. Proc. **891**, 71 (2007).
[28] B. Wilkins, M. Fluss, S. Kaufman, C. Gross, and E. Steinberg, Nucl. Instrum. Methods **92**, 381 (1971).
[29] E. K. Hulet, Phys. At. Nucl. **57**, 1099 (1994).
[30] O. B. Tarasov and D. Bazin, Nucl. Instrum. Methods Phys. Res., Sect. B **266**, 4657 (2008).
[31] P. Mosat, S. Antalic, F. Heßberger, D. Ackermann, B. Andel, M. Block, S. Hofmann, Z. Kalaninova, B. Kindler, I. Kojouharov, M. Laatiaoui, B. Lommel, A. Mistry, K. Nishio, J. Piot, B. Sulignano, and M. Vostinar, Acta Phys. Pol. B **49**, 605 (2018).
[32] S. Hofmann, W. Faust, G. Münzenberg, W. Reisdorf, P. Armbruster, K. Güttner, and H. Ewald, Z. Phys. A **291**, 53 (1979).
[33] K. H. Schmidt *et al.*, Z. Phys. A **316**, 19 (1984).
[34] F. Heßberger, S. Hofmann, D. Ackermann, V. Ninov, M. Leino, G. Münzenberg, S. Saro, A. Lavrentev, A. Popeko, A. Yeremin, and C. Stodel, Eur. Phys. J. A **12**, 57 (2001).
[35] B. Streicher, F. P. Heßberger, S. Antalic, S. Hofmann, D. Ackermann, S. Heinz, B. Kindler, J. Khuyagbaatar, I. Kojouharov, P. Kuusiniemi, M. Leino, B. Lommel, R. Mann, Š. Šáro, B. Sulignano, J. Uusitalo, and M. Venhart, Eur. Phys. J. A **45**, 275 (2010).
[36] J. S. Berryman, R. M. Clark, K. E. Gregorich, J. M. Allmond, D. L. Bleuel, M. Cromaz, I. Dragojević, J. Dvorak, P. A. Ellison, P. Fallon, M. A. Garcia, S. Gros, I. Y. Lee, A. O. Macchiavelli, H. Nitsche, S. Paschalis, M. Petri, J. Qian, M. A. Stoyer, and M. Wiedeking, Phys. Rev. C **81**, 064325 (2010).
[37] F. P. Heßberger, S. Hofmann, D. Ackermann, S. Antalic, B. Kindler, I. Kojouharov, P. Kuusiniemi, M. Leino, B. Lommel, R. Mann, K. Nishio, A. G. Popeko, B. Sulignano, S. Saro, B. Streicher, M. Venhart, and A. V. Yeremin, Eur. Phys. J. A **30**, 561 (2006).
[38] M. Vostinar, F. P. Heßberger, D. Ackermann, B. Andel, S. Antalic, M. Block, C. Droese, J. Even, S. Heinz, Z. Kalaninova, I. Kojouharov, M. Laatiaoui, A. K. Mistry, J. Piot, and H. Savajols, Eur. Phys. J. A **55**, 17 (2019).
[39] F. P. Heßberger, S. Hofmann, D. Ackermann, S. Antalic, B. Kindler, I. Kojouharov, P. Kuusiniemi, M. Leino, B. Lommel, R. Mann, K. Nishio, A. G. Popeko, B. Sulignano, S. Saro, B. Streicher, M. Venhart, and A. V. Yeremin, Eur. Phys. J. A **29**, 165 (2006).
[40] R. R. Chasman, I. Ahmad, A. M. Friedman, and J. R. Erskine, Rev. Mod. Phys. **49**, 833 (1977).
[41] P. Möller, A. Sierk, T. Ichikawa, and H. Sagawa, At. Data Nucl. Data Tables **109-110**, 1 (2016).